2008-09

Different origins of green-light photoluminescence emission in structurally ordered and disordered powders of calcium molybdate

Journal of Physical Chemistry A, Washington, DC, v. 112, n. 38, p. 8920-8928, Sept. 2008
http://www.producao.usp.br/handle/BDPI/49113

Different Origins of Green-Light Photoluminescence Emission in Structurally Ordered and Disordered Powders of Calcium Molybdate†

Valéria M. Longo,‡ Alberthmeiry T. de Figueiredo,§ Adaci B. Campos,§ Jose W. M. Espinosa,‡ Antônio C. Hernandes,|| C. A. Taft,⊥ Julio R. Sambrano,*,# José A. Varela,§ and Elson Longo§

LIEC, Departamento de Ciências e Engenharia de Materiais e Departamento de Química, UFSCar, 13565-905, São Carlos, SP, Brazil, LIEC, Instituto de Química, UNESP, 14801-970, Araraquara, SP, Brazil, IFSC, USP, P.O. Box 369, 13560-970, São Carlos, SP, Brazil, Centro Brasileiro de Pesquisas Físicas, Rua Dr. Xavier Sigaud, 150, Urca, 22290-180, Rio de Janeio, RJ, Brasil, and Grupo de Modelagem e Simulação Molecular, DM, UNESP, 17033-360, Bauru, SP, Brazil

Received: February 22, 2008; Revised Manuscript Received: April 22, 2008

A strong greenish-light photoluminescence (PL) emission was measured at room temperature for disordered and ordered powders of $CaMoO_4$ prepared by the polymeric precursor method. The structural evolution from disordered to ordered powders was accompanied by XRD, Raman spectroscopy, and TEM imagery. High-level quantum mechanical calculations in the density functional framework were used to interpret the formation of the structural defects of disorder powders in terms of band diagram and density of states. Complex cluster vacancies $[MoO_3 \cdot V_O^z]$ and $[CaO_7 \cdot V_O^z]$ (where $V_O^z = V_O^X, V_O^{\bullet}, V_O^{\bullet\bullet}$) were suggested to be responsible to the appearance of new states shallow and deeply inserted in the band gap. These defects give rise to the PL in disordered powders. The natural PL emission of ordered $CaMoO_4$ was attributed to an intrinsic slight distortion of the $[MoO_4]$ tetrahedral in the short range.

1. Introduction

Compounds of the tungstates and molybdates families with a scheelite-type structure have been extensively studied for a long time because of the technological interest of the natural luminescence properties. Ongoing intensive research interest with these materials can be attributed to their wide usage as phosphors, laser materials, and scintillation detectors.[1–4]

Calcium molybdate, $CaMoO_4$ (powellite, CM), is an important material within the scheelite family AXO_4, occurring with relatively large cations (A = Ca, Ba, Sr, Pb) and tetrahedral anions XO_4^{2-} (X = Mo, W).[5]

A variety of new fields for the application of these materials have emerged recently such as new generation of cryogenic detectors.[6] One reason for the particular importance of CM is based on the fact that this material is isostructural with $CaWO_4$ (scheelite) and exhibits sufficient light yield.[7] Thus, CM could be an excellent complementary material to calcium tungstate in a multitarget cryogenic search for dark matter. However, there are few studies about the luminescence and scintillation properties of CM.[7–10] More recently, CM is being studied as a material for cryogenic phonon scintillation detector applications.[11]

By using time-resolved spectroscopy, Leonelli and Brebner proposed a model to describe the luminescence process whereby electrons form small polarons that interact with holes to produce self-trapped excitons (STEs), with the recombination of STEs resulting in the visible emission, either immediately or after being trapped for a certain time by impurities and defects.[12,13]

As a result of previous studies of photoluminescence (PL) properties, we recently reported that two mechanisms were found to be responsible for PL emission in $CaWO_4$ and CM powders.[14] The first mechanism, in the disordered powders, was caused by oxygen complex vacancies $[MO_3 \cdot V_O^X]$, $[MO_3 \cdot V_O^{\bullet}]$, and $[MO_3 \cdot V_O^{\bullet\bullet}]$ (Kröger−Vink notation), where M = W or Mo, which leads to additional levels in the band gap. The second mechanism, in ordered powders, was caused by an intrinsic slight distortion of the $[WO_4]$ or $[MoO_4]$ tetrahedral.

In this work, a theoretical approach was given to the experimental PL results of the green-light emission of CM. Three disorder-type simulations were made in the crystalline (ordered) tetragonal unit cell as follows: in the network former (Mo), in the network modifier (Ca), and in the network former−modifier (Mo/Ca). These theoretical simulations should allow the demonstration of how different structural intrinsic defects contribute in the disordered systems and give rise to specific states in the forbidden gap leading to different electronic transitions and consequentially different color-light emissions. On the experimental side, a number of complementary characterization techniques were used such as Raman spectroscopy, optical absorption spectroscopy, and PL spectroscopy with two different wavelengths in order to obtain a clearer physical picture underlying the luminescence behavior of the CM scheelite ordered and disordered structure.

2. Experimental Section

Ordered and disordered CM powders were synthesized by the polymeric precursor method.[15] Experimental details of the preparation of the powders are described elsewhere.[16] The powders were annealed in the temperature range of 350 to 700 °C during 4 h in an oxygen atmosphere.

† Part of the special section for the "Symposium on Energetics and dynamics of Molecules, Solids and Surfaces".

* Corresponding author. E-mail: sambrano@fc.unesp.br.
‡ Departamento de Ciências e Engenharia de Materiais e Departamento de Química.
§ Instituto de Química.
|| USP.
⊥ Centro Brasileiro de Pesquisas Físicas.
Grupo de Modelagem e Simulação Molecular.

10.1021/jp801587w CCC: $40.75
Published on Web 07/01/2008

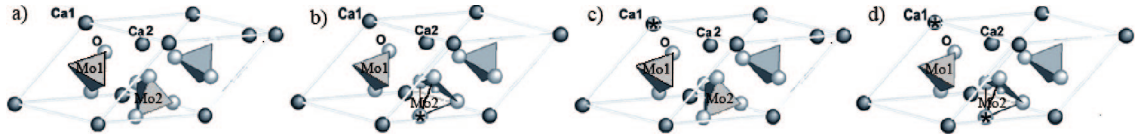

Figure 1. (a) Ordered model of symmetric CM-o. (b) Asymmetric CM-f model of network former displacement. (c) Asymmetric CM-m model of network modifier displacement. (d) Asymmetric model of network former and modifier displacement CM-fm.

The powder samples were structurally characterized by the X-ray diffraction (XRD) method by using a Rigaku D/max −2500 and a Cu kα radiation source. The diffraction patterns were recorded by using a -2θ configuration (θ is the diffraction angle). Two kinds of powders have to be distinguished for a better understanding of this work: the first one, structurally disordered, the thermal treatment of which was done below the crystallization temperature and the structurally ordered samples, in which crystallization has been obtained. The spectral dependence of the optical absorbance of the ordered and disordered powders was measured at room temperature in the total reflection mode by using a Cary 5G spectrophotometer. Raman spectra were recorded on a RFS/100/S Bruker FT-Raman spectrometer with a Nd:YAG laser providing excitation light at 1064 nm.

Specimens for transmission electron microscopy (TEM) of CM were subjected to ethanolic dispersion into an ultrasonic (ultrassonic cleaner 1440D) for 4 min, dispersed in a Cu grid with 2 mm diameter, and dried in air. TEM images were taken at an accelerating voltage of 200 kV with a Philips CM200 instrument.

The PL of the powder measurements were taken with a Thermal Jarrel-Ash Monospec 27 monochromator and a Hamamatsu R446 photomultiplier. The 350.7 nm excited wavelength of a krypton ion laser (Coherent Innova) was used, with the nominal output of the laser kept at 200 mW. For the 488 nm wavelength excitation, an argon ion laser U1000 Jobin-Yvon double monochromator coupled to a cooled GaAs photomultiplier and a conventional photon-counting system was used, with the nominal output power of the laser kept at 20 mW. All the measurements were taken at room temperature.

3. Periodic Models and Computing Method

Powellite CM crystallizes in a tetragonal structure (space group $I4_1/a$, C_{4h}^6 symmetry). In this structure, the molybdenum atoms are surrounded by four oxygen atoms in a tetrahedral configuration, and calcium atoms are surrounded by eight oxygens in a pseudo cubic configuration to represent the ordered CM-o. This model can be designated as $[MoO_4]-[MoO_4]$, because each molybdenum atom is surrounded by four oxygen atoms in a C_{4h}^6 configuration. This results in 12 atoms in the unit cell presented in Figure 1a. The cell and atomic position parameters used in the calculation of the ordered and disordered structures ($a = 5.2259$ Å and $c = 11.4419$ Å) are taken from results of Rietveld refinements.

Experimental X-ray absorption near-edge structure results[16] of the disordered phase of $SrTiO_3$ revealed the coexistence of two types of environments for titanium atoms, namely, 5-fold titanium coordination $[TiO_5 \cdot V_O^Z]$, $V_O^Z = V_O^X$, $V_O^{\bullet}$, $V_O^{\bullet\bullet}$ and 6-fold titanium coordination $[TiO_6]$. On the basis of this information, it was assumed that before the powders become completely crystallized, the structure is composed of a random mixture of $[MoO_4]$ and $[MoO_3 \cdot V_O^Z]$ complex clusters linked by Ca. Three unit cells were therefore created to stand for the disordered models. Starting from the previous CM-o model, the network former Mo2 atoms were shifted by 0.3 Å in the direction opposite to that of the starred oxygens of Figure 1b, thereby breaking the bond. Because of their asymmetry in the network former, these new disordered periodic models are called CM-f. The Mo2 atoms are now surrounded by three oxygen atoms in this first coordination sphere.

The network modifier disorder (CM-m) was modeled by shifting the Ca1 from its previous position in the modifier unit cell. This displacement causes asymmetries in the unit cell, where Ca1 is now surrounded by seven oxygens $[CaO_7 \cdot V_O^Z]$, whereas Ca2 is surrounded by eight oxygens $[CaO_8]$, as in the case of CM-o. Therefore, this asymmetric CM model, CM-m, represents the disorder in the network modifier material. This structure can be designated as $[CaO_8]-[CaO_7 \cdot V_O^Z]$, depending on the displacement of the calcium (Figure 1c).

Finally, the network former and modifier disorder (CM-fm) was modeled at the same time by shifting both molybdenum and calcium in the same way as described above. This displacement produces asymmetries in the unit cell, where Mo2 is now surrounded by three oxygens, whereas the other three Mo are surrounded by four oxygens, Ca1 is surrounded by seven oxygens, and Ca2 is surrounded by eight oxygens. Therefore, in this asymmetric CM model, CM-fm represents the disorder in the network former and modifier material. This structure can be designated as $[MoO_4]-[MoO_3 \cdot V_O^Z]$ and $[CaO_8]-[CaO_7 \cdot V_O^Z]$ (see Figure 1d). With these models, the effects of different structural disorders can be separately evaluated in terms of the electronic structure.

Periodic DFT quantum-mechanical calculations performed with the B3LYP hybrid functional[18,19] have been carried out by means of the CRYSTAL03[20] computer code. This functional has already been successfully employed in studies of the electronic and structural properties of the bulk and surfaces of various compounds.[21]

The atomic centers have been described by the basis sets Mo,[22] Ca (86-511d3G),[23] and O (6-31G*).[23] K-points sampling was chosen as 36 points within the irreducible part of the Brillouin zone. The XcrysDen program was used to design the band structure diagrams.[24]

Our objective with this modeling is not to represent the exact reality of the disordered structures but to offer a simple scheme that could facilitate the comprehension of the effects of structural deformation on the electronic structure without completely suppressing the geometry of the cell, which is useful for periodic calculation. These models can be useful to represent different degrees of order−disorder in matter and structural intrinsic defects that result from the presence of $[MoO_4]-[MoO_3 \cdot V_O^Z]$ and/or $[CaO_8]-[CaO_7 \cdot V_O^Z]$ complex clusters.

4. Results and Discussion

Figure 2a,b ilustrates the TEM images of CM annealed at 600 °C. The morfology of the polycrystalline particles seems to be spherical and well defined. The the particles have a diameter between 33 to 227 nm are composed by aglomerates of polycrystalline particles. In addition, the corresponding SAD

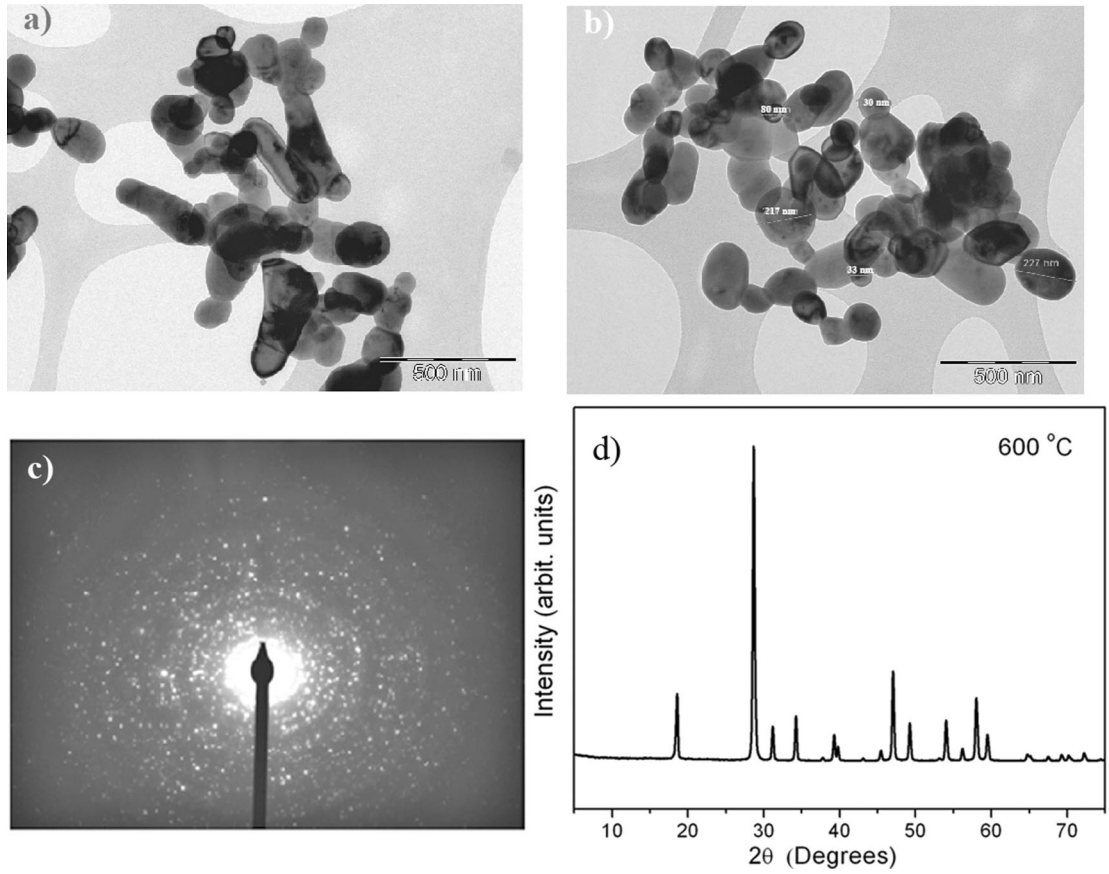

Figure 2. CM powders annealed at 600 °C. (a) Typical TEM image. (b) Particles diameter ranging from 33 to 227 nm. (c) SAD pattern of sample. (d) XRD of single phase of CM.

pattern (Figure 2c) confirms that the structure has a morfology of the polycrystalline particles. The XRD pattern presented in Figure 2d shows that the CM powder is ordered at long range with a single phase.

In Figure 3 is presented the TEM and XRD of CM annealed at 700 °C.

Figure 3a shows that the morfology of the polycrystalline particles are still spherical and well defined. The particles have a diameter between 70 to 251 nm and are composed of aglomerates of polycrystalline particles as in case of the powder annealed at 600 °C but slightly larger. Figure 3b shows the surface of the particle in more detail. This image is characteristic of cyrstalline morphology. The corresponding SAD pattern (Figure 3c) shows the structure of a single particle. The XRD pattern presented in Figure 3d shows the diffraction peaks characteristics of CM. They can be indexed in a scheelite tetragonal unit cell with space group $I4_1/a$ in C_{4h}^6 symmetry (JCPDS- 41-1431).

Figure 4 shows the Raman spectra of CM samples annealing at 600 and 700 °C.

The scheelite crystal structure has C_{4h}^6 symmetry at room temperature. The internal vibration corresponds to the oscillations inside the MoO_4 molecular group. The external or lattice phonons correspond to the motion of the Ca cation and the rigid molecular unit (translational modes).[25] Vibrational modes characteristic of the scheelite phase in the tetrahedral structure were observed at 600 and 700 °C. The sample treated at 700 °C presents several peaks referring to the Raman-active internal modes of MoO_4 tetrahedra: υ_1 (A_g), υ_3 (B_g), υ_3 (E_g), υ_4 (E_g), υ_4 (B_g), υ_2 (B_g), υ_2 (A_g), R (A_g), R (E_g) and external T (B_g E_g E_g) mode. This structure is well organized in the short and long range. However, the powder annealed at 600 °C does not show the T (E_g) external Raman modes. In the case of disordered structures, the occurrence of Raman modes activation that are forbidden[26] is possible. In the case of the powder annealed at 600 °C in 127, 155, 664, and 816 cm^{-1}, there is occurrence of these modes, indicating that there is short-range disorder in the [MoO_4] cluster (internal modes) and in the Ca lattice (external modes). The results of the XRD taken at room temperature showed a long-range order or periodicity for CM at this temperature (Figure 2d). The difference between X-ray and Raman results can be explained by the fact that X-ray probes the overall long-range order, whereas Raman scattering probes the short-range structural order.

The absorbance spectral dependence of the CM powder annealed at 450, 500, 600, and 700 °C is shown in Table 1. The optical energy band gap is related to the absorbance and the photon energy by the following equation:

$$h\nu\alpha \propto (h\nu - E\mathrm{opt}_g)^2 \qquad (1)$$

were α is the absorbance, h is the Planck constant, ν is the frequency, and E^{opt}_g is the optical band gap.[27] The sample annealed at 700 °C presents a well-defined interband transition with quasi vertical absorption front, typical of semiconductor crystalline materials. However, the typical shape of the spectra of the powders annealed at 450, 500, and 600 °C is that of structurally disordered semiconductors with absorption tails below the exponential part of the edge. Wood and Tauc[27] associated these absorption tails with localized states in the band gap, interband states linked to defects in the structure. In this sense, the well-ordered powder has a band gap of 4.0 eV, and the most disordered powder, annealed at 450 °C, has a band gap of 2.9 eV with defects deeply inserted in the band gap.

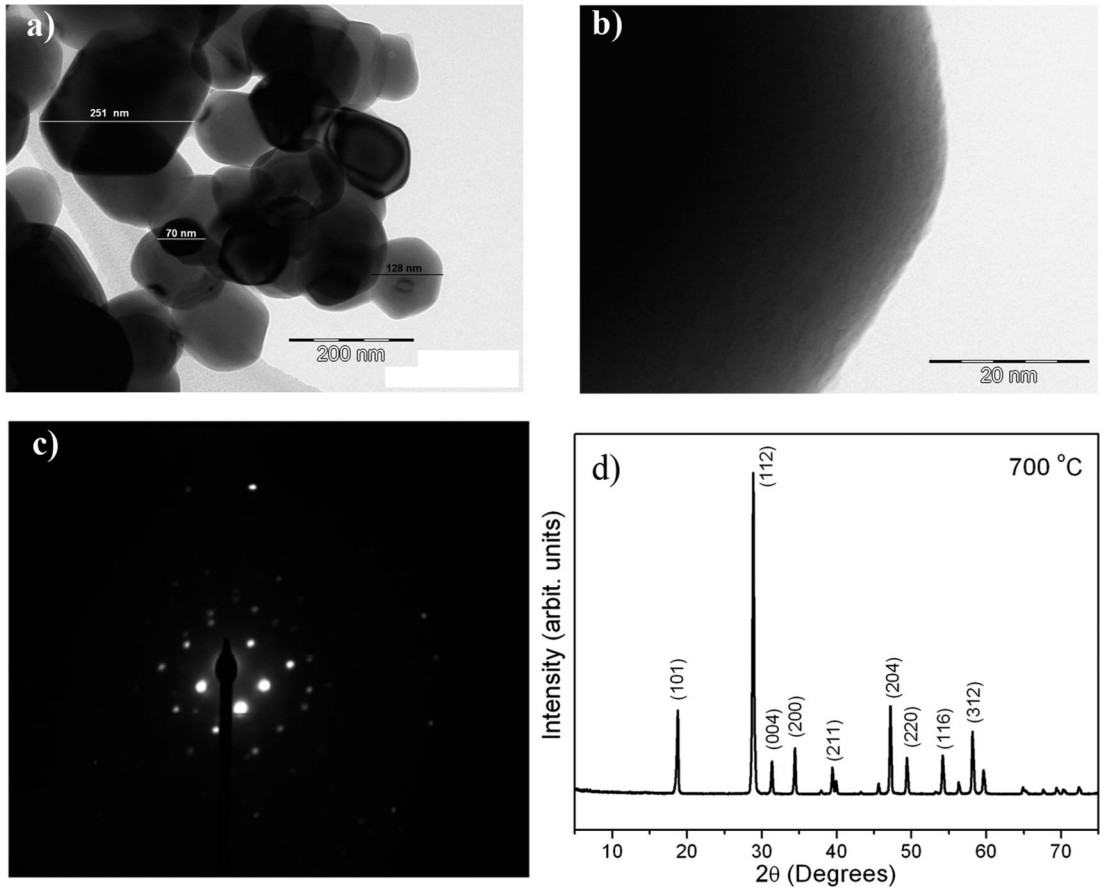

Figure 3. CM powders annealed at 700 °C. (a) Typical TEM image. (b) Particles diameter ranging from 70 to 251 nm. (c) SAD pattern of on single particle. (d) XRD of single phase of CM.

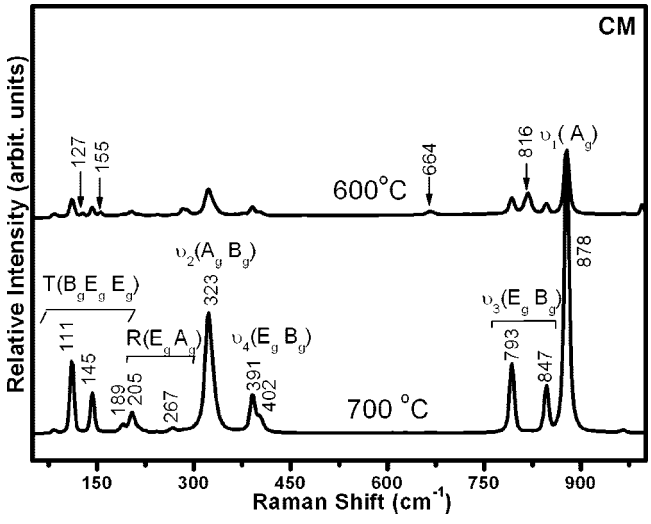

Figure 4. Room-temperature depolarized Raman spectra of powders annealed at 600 and 700 °C for 4 h.

TABLE 1: Spectral Dependence of the Absorbance for the CM Powders Annealed in Range from 450 to 700 °C

annealing temperature (°C)	experimental gap (eV)
450	2.9
500	3.7
600	4.2
700	4.7

By using the theoretical models to facilitate the comprehension of our experimental result, the differences in the electronic structure are analyzed, whereas it is convenient to make reference to band structure parameters which can be compared to each other independently of the crystal space group. Figure 5 shows the band structure of CM-o, CM-f, CM-m, and CM-fm models (0.3 Å dislocation).

Figure 5a depicts the calculated band structure of bulk CM-o. The top of the valence band (VB) as well as the bottom of the conduction band (CB) are at the Γ point. The minimum calculated direct gap is 5.15 eV, which is close to the experimental gap of ordered powder annealed at 700 °C deduced from the optical absorption edge, which was found to be 4.7 eV (see Table 1).

The calculated band structure of bulk CM-f is depicted in Figure 5b. The gap is direct at the Γ point and is found to be 3.98 eV. The molybdenum, which is the lattice former, ideally tends to bond with four oxygen atoms, but before it reaches this ideal configuration, there are various coordination numbers for Mo in the structure. Before it becomes crystallized, the structure is a mixture of MoO_x complex clusters (x = mostly 3 and 4) intercalated with Ca atoms. For higher annealing temperatures, the [MoO_4] complex is more frequent, and there is more structural order. Previous Raman spectroscopic measurements[2] on the structurally disordered $SrWO_4$ indicated that the former molybdenum lattice organizes before the strontium lattice modifier. We believe that for the CM structure, the same process takes place and that this model represents only the electronic states derived from disorder in the former lattice and cannot be compared with experimental powder. We do not expect disorder only in the network former, but this displacement induces new electronic states that are deeply inserted in band gap.

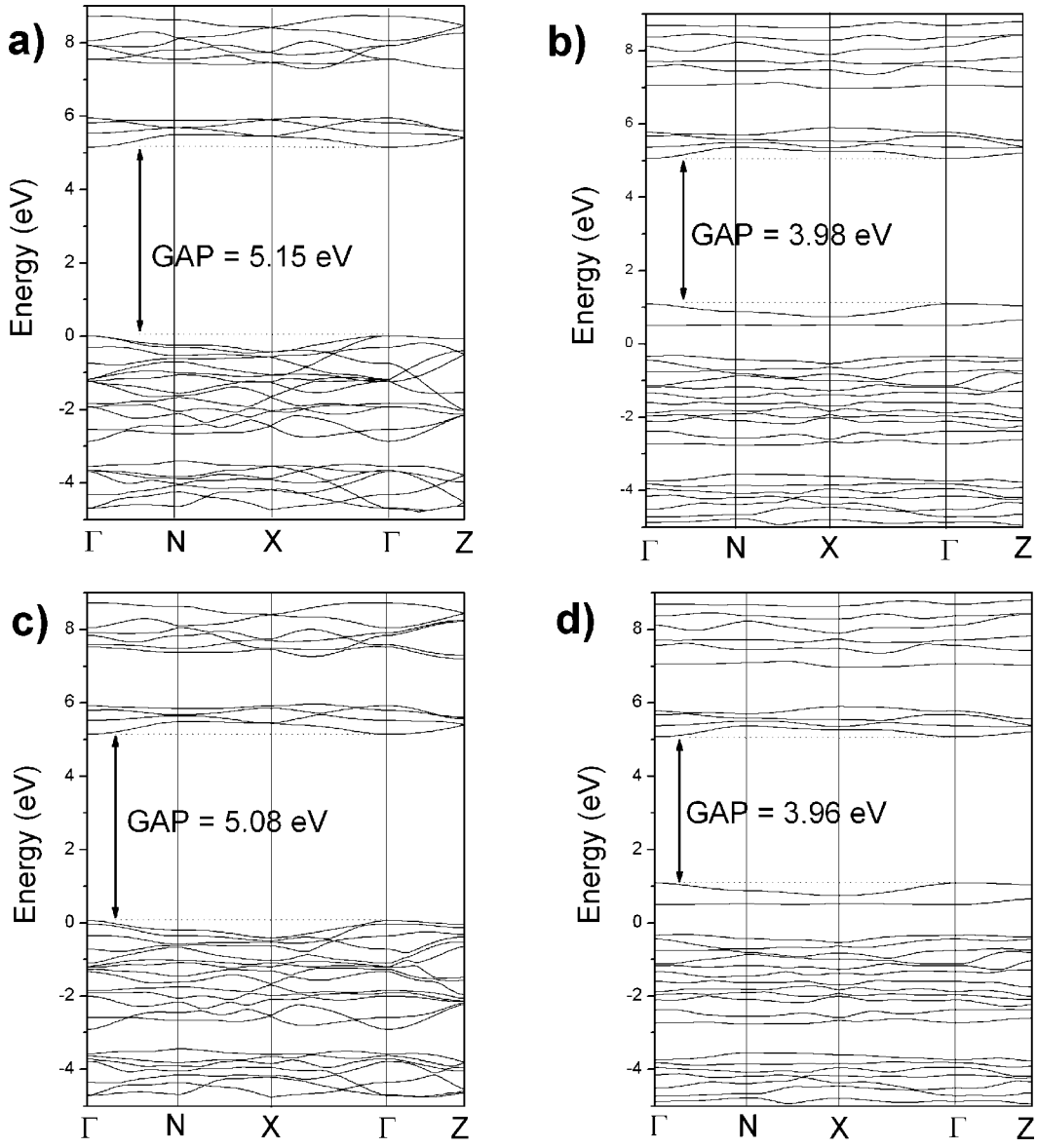

Figure 5. Calculated energy band structures for (a) CM-o, (b) CM-f, (c) CM-m, and (d) CM-fm.

The calculated band structures of CM-m and CM-fm are reported, respectively, in Figure 5c and d. The direct minimum theoretical gap for the CM-m Γ point is found to be 5.08 eV and was related to powder annealed at 600 °C (4.2 eV) (see Table 1). It can be said that the new states formed are shallow because the band gap is just slightly smaller in relation to that of the CM-o model. For the CM-fm model, the calculated band gap was 3.96 eV, which represents the major disorder of the lattice and disordered powder annealed at 450 °C (2.9 eV) and represents the defects most deeply inserted in band gap. These results indicate congruence between the experimental and theoretical data.

For CM-o (Figure 5a), the VBs derive from $2p_x$, $2p_y$, $2p_z$ orbitals of O atoms. They are separated by an indirect gap from the first CB, which derives from transition-metal molybdenum ($4d_{xy}$, $4d_{xz}$, $4d_{yz}$) atomic orbitals, designated as t_{2g} by comparison with the [MoO_4] regular cluster. Above these six bands are four Mo ($4d_{x^2-y^2}$ and $4d_{z^2}$) character bands designated as e_g. For the displaced models (CM-f, CM-m, and CM-fm), although the VB is globally composed of O ($2p_x$, $2p_y$, $2p_z$) character states, the top depends mainly on the oxygen (O*) that has been displaced. The CB is composed of the 4d states of molybdenum in an apparently random splitting of bands (Figure 5b−d).

The density of states (DOS) for CM-o, CM-f, CM-m, and CM-fm are shown in Figure 6a−d. For the CM-o model, the upper VB is mainly made of the O (2p) states equivalentetly distributed on each oxygen. The projections on oxygens and molybidenium reveal that the upper VB states are mostly nonligand states in relation to the Mo−O bonds. The strong covalent hybridization between the *2p* O and 4d Mo levels is clearly visible in both the upper CB band and the lower VB. The projected DOS on Ca atom appears in the CB with the 3d Ca states (not shown). The interactions between Ca and Mo/O are small.

For the CM-f model, the upper VB is predominately made of the O (2p) states with new states formed above 0 eV. These new states are mostly formed by the 2p O* nonbonding character of the oxygen that looses connection with Mo2 (see Figure 1b). The lower CB is also made of 4d Mo states. These new states created below the CB are due to the $4d_{z^2}$ and $4d_{x^2-y^2}$ orbitals of the shifted molybdenum atom (Mo2). The interaction between oxygen and molybdenum is also visible.

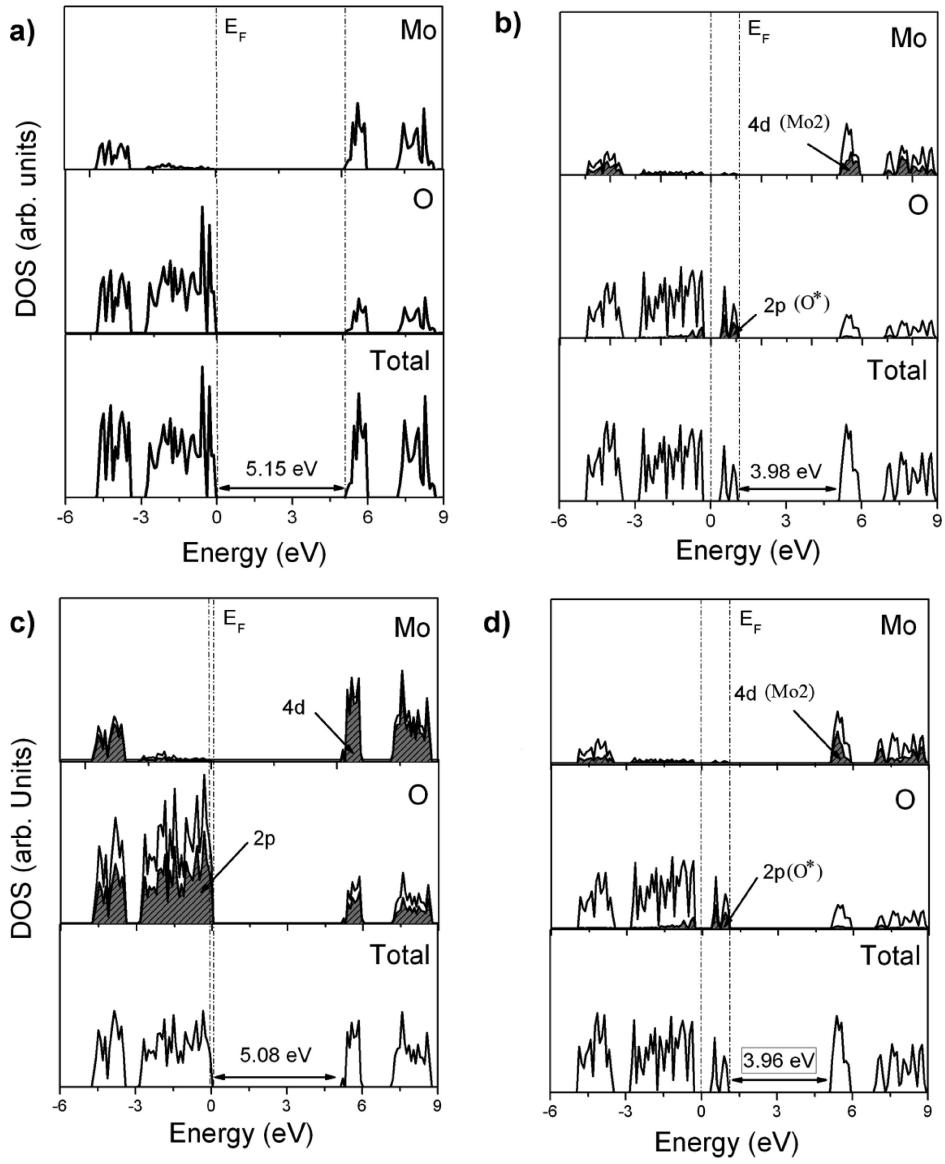

Figure 6. Total and atom-projected DOS for (a) CM-o, (b) CM-f, (c) CM-m, and (d) CM-fm models.

In the CM-m case (Figure 6c), the upper VB are composed mainly of the 2p oxygens state equivalentetly distributed on each oxygen. However, there are small changes of VB states and consequent reduction of band gaps. The lower CB is also made of 4d Mo states. The contribution of 3d Ca levels are almost negligible.

The CM-fm structure is analogous to the CM-f model indicating that the network former creates a split of degeneracy greater than that of the network modifier (Figure 6d). The Mo−O covalent bond creates a limited Mo (4d) contribution in the O (2p) region as well as a weak O (2p) contribution to the Mo (4d) region.

The decrease of the band gap in structurally disordered powder can be attributed to defects and/or local bond distortion which yield localized electronic levels in the band gap of this material. However, the tail observed in the UV−vis spectral measurements of disordered powders only shows the presence of defects and consequently localized electronic levels in the forbidden band gap but cannot indicate the nature of these defects.

The ordered and disordered theoretical models indicated that disorder in the former lattice produce deep defects in the band gap, whereas disorder in the modifier lattice produces shallow defects in the band gap.

Complex oxygen vacancies are dominant defect in undoped CM. The creation of intrinsic n-type defects, such as oxygen complex $[MO_3 \cdot V_O^z]$ or $[CaO_7 \cdot V_O^z]$, is more favorable than that of intrinsic p-type defects, such as Mo or Ca vacancies (V_{Mo} or V_{Ca}).

The shallow and deep defects can be modulated by the oxygen displacement in disordered powders of CM by the presence of V_O^X, $V_O^{\bullet}$, and $V_O^{\bullet\bullet}$species that are linked to the $[MoO_3]$-yielding complex clusters. These complex clusters in molybidates can occur in three different charge states: the $[MoO_3 \cdot V_O^X]$ complex states, which presents two paired electrons $\underline{\uparrow\downarrow}$ and is neutral relative to the lattice, the singly ionized $[MoO_3 \cdot V_O^{\bullet}]$ complex state, which has one unpaired electron $\underline{\uparrow}$, and the $[MoO_3 \cdot V_O^{\bullet\bullet}]$ complex state, which did not trap any electrons and is double positively charged with respect to the lattice. Other electrons and holes may be trapped by intrinsic crystal defects in the network modifier $[CaO_7 \cdot V_O^z]$ complex cluster. These oxygen vacancies induce new energy levels in the band gap, as previously discussed regarding the electronic band structure, and

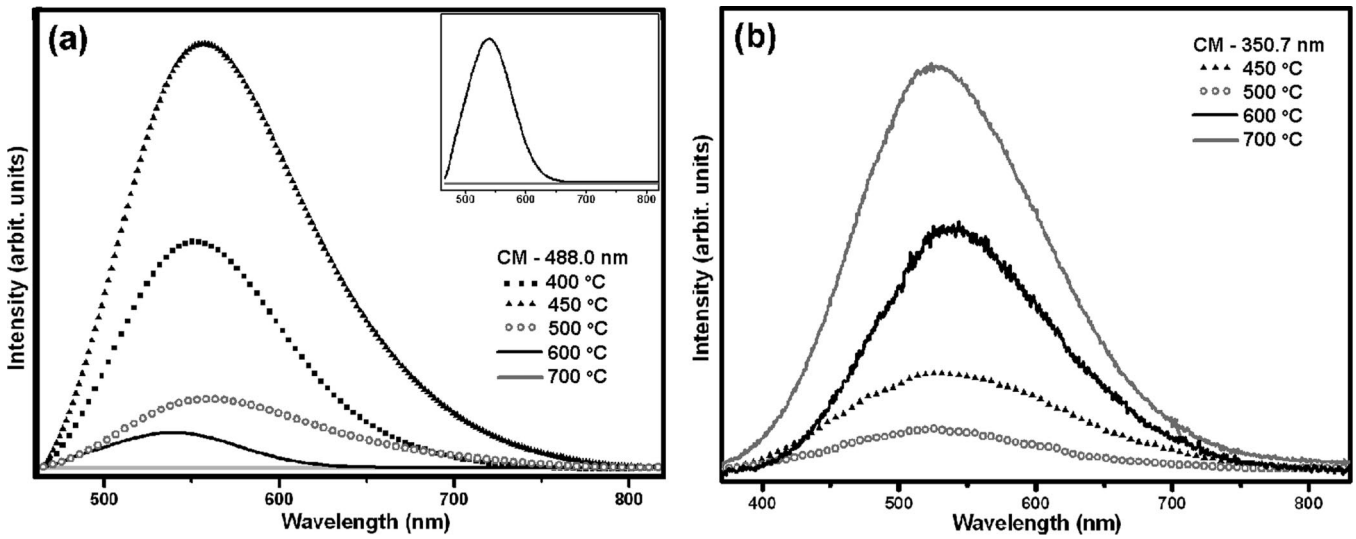

Figure 7. PL spectra recorded at room temperature for the CM powders. (a) Excitation wavelength of argon ion laser at 488 nm. (b) Excitation wavelength of a krypton ion laser at 350.7 nm.

can be attributed to the calcium−oxygen or molybdenum−oxygen complex vacancy centers.

Figure 7 illustrates PL spectra recorded at room temperature for the CM powders with heat treatment at 400, 450, 500, 600, and 700 °C for two different excitation wavelengths, that is, 350.7 nm wavelength excitation of a krypton ion laser and 488 nm wavelength excitation of an argon ion laser.

The profile of the emission band is typical of a multiphonon and multilevel process, that is, a system in which relaxation occurs by several paths, involving the participation of numerous states within the band gap of the material.

Quantum mechanical calculations of dislocated $[MoO_4]$ and/or $[CaO_8]$ complex clusters indicate that localized states generated in the band gap reduces the gap energies. When the structural order increases, the gap energy increases. These observations confirm the fact that PL is directly associated with the localized states existing in the band gap and that the degree of order−disorder changes these localized states.

The strength of the electron−phonon interaction can be attributed to the difference between the excitation and the emission maximum (Stokes shift). The Stokes shifts are greatest at a wavelength of 350.7 nm, but the maximum emission in the two wavelengths and in all the annealing temperatures are in the range of the green of visible light (500−570 nm).

There are significant differences in the PL emission when comparing the two excitation wavelength as a function of the annealing temperatures. When the ordered powder annealed at 700 °C was excited with a 488 nm wavelength of an argon ion laser (insert Figure 7a), its intensity dropped to almost zero. This suggests that when the crystallization temperature was reached, the energy of 2.54 eV (488 nm) was unable to attain the lowest position of the localized levels in the band gap of this sample, and PL emission was not observed. At 600 °C, when the powdered sample indicated long-range order until disorder at short range, the PL emission was low but present. The rearrangement of the lattice when the annealing temperature changes from 600 to 700 °C was clearly detected through PL experimental measurements and is a strong indication that this measurement is highly sensitive to structural changes.

The powders annealed at 400, 450, and 500 °C indicate a greenish luminescence and are structurally disordered at short and long range as observed by XRD and Raman spectroscopy. The deep and shallow defects in the band gap present in the disordered powders yields a wide band of PL emission in the visible spectra of light. In this respect, each color represents a different type of electronic transition and is linked to a specific structural arrangement. The blue and green emissions are thus attributed to shallow defects in the band gap and to a more ordered structure, whereas the yellow and red emissions are linked to defects deeply inserted in the band gap and to a greater disorder in the lattice. It can be inferred that an increased disorder in the lattice is associated with the presence of $[MoO_3 \cdot V_O^{\bullet\bullet}]$ and $[MoO_3 \cdot V_O^{\bullet}]$ complex clusters and that these complex defects are deeply inserted in the band gap, leading to yellow−red PL emission. On the other hand, $[CaO_7 \cdot V_O^{\bullet\bullet}]$ and $[CaO_7 \cdot V_O^{\bullet}]$ complex clusters are linked to shallow defects in the band gap and lead to a more energetic PL emission (blue−green light). Increasing the lattice order causes these complex vacancies and the PL emission to disappear in the 488 nm excitation line.

In our model, the wide band model,[28] the most important events occur before excitation, that is, before the arrival of the photon. Deep and shallow oxygen complex clusters generate localized states in the band gap and nonhomogeneous charge distribution in the cell, thereby allowing electrons to become trapped. The localized levels are energetically distributed so that various energies are able to excite the trapped electrons.

Before donor excitation, a hole in the acceptor state and an electron in the donor state are created according to the following equations:

$$[MoO_4]^X + [MoO_3 \cdot V_O^X] \rightarrow [MoO_4]' + [MoO_3 \cdot V_O^{\bullet}] \quad (2)$$

$$[MoO_4]^X + [MoO_3 \cdot V_O^{\bullet}] \rightarrow [MoO_4]' + [MoO_3 \cdot V_O^{\bullet\bullet}] \quad (3)$$

$$[CaO_8]^X + [CaO_7 \cdot V_O^X] \rightarrow [CaO_8]' + [CaO_7 \cdot V_O^{\bullet}] \quad (4)$$

$$[CaO_8]^X + [CaO_7 \cdot V_O^{\bullet}] \rightarrow [CaO_8]' + [CaO_7 \cdot V_O^{\bullet\bullet}] \quad (5)$$

where $[MoO_4]'$or $[CaO_8]'$ are donors, $[MoO_3 \cdot V_O^{\bullet}]$ or $[CaO_7 \cdot V_O^{\bullet}]$ are donors/acceptors, and $[MoO_3 \cdot V_O^{\bullet\bullet}]$ or $[CaO_7.V_O^{\bullet\bullet}]$ are acceptors.

These equations suggest that the oxygen-vacancy-trapped electron in the VB is a necessary requirement for the transition of a VB hole in the CB. This means that most of the electrons around the oxygen vacancies are released, and therefore, such

oxygen vacancy complex sites are, in principle, positively charged. Moreover, oxygen vacancies tend to trap photogenerated electrons. The charge transfer that occurs as proposed in eqs 1–4 creates electron and hole polarons that can be designated as bipolarons.

In the complex, the $[MoO_4]'$ or $[CaO_8]'$ clusters act as electron donors, whereas the vacancy complexes $[MoO_3 \cdot V_O^{\bullet}]$ and $[CaO_7 \cdot V_O^{\bullet}]$ tend to trap electrons and/or holes and $[MoO_3 \cdot V_O^{\bullet\bullet}]$ or $[CaO_7.V_O^{\bullet\bullet}]$ act as electron traps. After excitation of the photon, the recombination and decay process should follow various hypotheses presented in the literature.[12,13,29,30]

When the 350.7 nm excitation wavelength was used (Figure 7b), the maximum PL emission was obtained in the ordered powder annealed at 700 °C. This is a strong indication that a more energetic wavelength could excite other populations of self-trapped electrons present in the well-ordered powders. The greenish emission, in this case, was attributed to periodic short-range order (interaction between Mo−O).

Disorder in materials can be manifested in many ways. Examples are vibrational, spin and orientation disorder (all referred to a periodic lattice), and topological disorder. The latter is the type of disorder associated with the structure of glassy and amorphous solids in which the structure cannot be defined in terms of a periodic lattice. PL is a powerful probe of certain aspects of short-range order in the range 2−5 Å and medium range 5−20 Å, such as clusters, where the degree of local order is such that structurally inequitable sites can be distinguished because of their different types of electronic transitions and are linked to a specific structural arrangement.

Numerous papers have discussed the PL behavior of crystalline $CaWO_4$ and CM. When excited by short-wavelength ultraviolet radiations at room temperature, they present a predominantly blue-greenish emission band, which is commonly attributed to the WO_4 tetrahedron.[31–33] There is also a green emission band, the origin of which is still controversial, because it has already been attributed to WO_3 defect centers associated with oxygen vacancies[34] as well as to intrinsic transitions in the WO_4^{2-} complex.[35] Lou and Cocivera[35] mention the existence of a red emission band under longer wavelength excitations. According to the literature, $[WO_3]'$ vacancy-containing complex anions associated with a defect in the sublattice $[WO_3]'-Ca^{\bullet\bullet}$ complexes have been identified by ESR analysis.[36]

Therefore, it can be attributed to the greenish PL emission of the well-ordered powder at 700 °C to the intrinsic slightly distorted $[MoO_4]$ tetrahedron in short range, according to previous results reported in the literature.[31–33] However, we note that the excitation line of 350.7 nm (3.54 eV) is lower than the band gap experimentally measured (4.7 eV) in ordered powders. Then, this slight disordered tetrahedron must induce additional levels in the band gap. In order to determine the effect of this intrinsic natural disorder of the tetrahedron that leads to PL emission, more accurate experimental and theoretical analyses have to be done in the short- and medium-range order. The experimental analysis that can shed light in the PL emission light observed in ordered powders have to be done with exited states during the exited process. The theoretical models should investigate slight disorder in the tetrahedral (short-range order) and angles between tetrahedral (medium-range order).

5. Conclusions

Ultrafine CM powders were synthesized by a soft chemical process. The structural evolution of disorder to order of the powders was analyzed in the light of XRD, Raman spectroscopy, and TEM imaging. The results indicate that the CM powder annealed at 600 °C is ordered at long range and disordered at short range, and the powder annealed at 700 °C is ordered at short and long range. The calculated band gap confirms the UV−vis results and indicates the changes in electronic states produced by structural displacements in network former and modifier. As the structural order increases, so does the gap energy. The structural evolution from disorder to order occurs first in the network former and then in the network modifier.

The two excitation lines used for the PL measurements enabled us to understand the various populations of levels that already exist in the disordered powder, which was also confirmed by the periodic DFT calculation.

The increased disorder in the lattice was associated with the presence of $[MoO_3 \cdot V_O^{\bullet}]$ and $[MoO_3 \cdot V_O^{\bullet\bullet}]$ complex clusters (disorder in the network former) and attributed to defects deeply inserted in the band gap. In this sense, the $[CaO_7 \cdot V_O^{\bullet}]$ and $[CaO_7 \cdot V_O^{\bullet\bullet}]$ complex clusters (disorder in the network modifier) were associated with shallow defects in the band gap.

Two mechanisms were found to be responsible for PL emission in CM powders, in this work. The first one, in the disordered powders, was caused by oxygen complex vacancies $[MoO_3 \cdot V_O^{X}]$, $[MoO_3 \cdot V_O^{\bullet}]$, and $[MoO_3 \cdot V_O^{\bullet\bullet}]$, which leads to additional levels in the band gap and was confirmed by simulations. The second mechanism, in ordered powders, was attributed to an intrinsic slight distortion of the $[MoO_4]$ tetrahedral in the short range.

Acknowledgment. The authors would like to thank the Brazilian research financing institutions FAPESP/CEPID, CNPq, and CAPES for their funding of this work. The constructive comments of the referees are gratefully acknowledged.

References and Notes

(1) Cho, W. S; Yashima, M.; Kakihana, M.; Kudo, A.; Sakata, T.; Yoshimura, M. *J. Am. Ceram. Soc.* **1997**, *8* (3), 765.

(2) Anicete-Santos, M.; Picon, F. C.; Escote, M. T.; Leite, E. R.; Pizani, P. S; Varela, J. A.; Longo, E. *Appl. Phys. Lett.* **2006**, *88*, 211913.

(3) Klassen, N.; Shmurak, S.; Redkin, B.; Ille, B.; Lebeau, B.; Lecoq, P.; Schneegans, M. *Nucl. Instrum. Methods Phys. Res. A* **2002**, *486*, 431.

(4) Danevich, F. A.; Georgadze, A.; Sh.; Kobychev, V. V.; Kropyvyansky, B. N.; Kuts, V. N.; Nikolaiko, A. S.; Tretyak, V. I.; Zdesenko, Y. *Phys. Lett. B* **1995**, *344*, 72.

(5) Sleight, W. *Acta Crystallogr. B* **1972**, *28*, 2899.

(6) Meunier, P.; Bravin, M.; Bruckmayer, M.; Giordano, S.; Loidl, M.; Meier, O.; Pröbst, F.; Seidel, W.; Sisti, M.; Stodolsky, L.; Uchaikin, S.; Zerle, L. *Appl. Phys. Lett.* **1999**, *75*, 1335.

(7) Mikhailik, V. B.; Kraus, H.; Miller, G.; Mykhaylyk, M. S.; Wahl, D. *J. Appl. Phys.* **2005**, *97*, 083523.

(8) Mikhailik, V. B.; Kraus, H.; Wahl, D.; Mykhaylyk, M. S. *Phys. Status Solidi B* **2005**, *242*, R17.

(9) Mikhailik, V. B.; Kraus, H.; Itoh, M.; Iri, D.; Uchida, M. *J. Phys.: Condens. Matter.* **2005**, *17*, 7209.

(10) Groenink, J. A.; Hakfoort, C.; Blasse, G. *Phys. Status Solidi A* **1979**, *54*, 329.

(11) Senyshyn, A.; Kraus, H.; Mikhailik, V. B.; Vasylechko, L.; Knapp, M *Phys. Rev. B* **2006**, *73*, 014104.

(12) Leonelli, R.; Brebner, J. L. *Solid State Commun.* **1985**, *54*, 505.

(13) Leonelli, R; Brebner, J. L. *Phys. Rev. B* **1986**, *33*, 8649.

(14) Campos, A. B.; Simões, A. Z.; Longo, E.; Varela, J. A.; Longo, V. M.; de Figueiredo, A. T.; De Vicente, F. S.; Hernandes, A. C. *Appl. Phys. Lett.* **2007**, *91*, 051923.

(15) Kakihana, M.; Yoshimura, M. *Bull. Chem. Soc. Jpn.* **1990**, *72*, 1427.

(16) Maurera, M. A. M. A.; Souza, A. G; Soledade, L. E. B.; Pontes, F. M.; Longo, E.; Leite, E. R.; Varela, J. A. *Mater. Lett.* **2004**, *58*, 727.

(17) Pontes, F. M.; Longo, E.; Leite, E. R.; Lee, E. J. H.; Varela, J. A.; Pizani, P. S.; Campos, C. E. M.; Lanciotti, F.; Mastelaro, V.; Pinheiro, C. D. *Mater. Chem. Phys.* **2003**, *77*, 598.

(18) Lee, C. T.; Yang, W. T.; Parr, R. G. *Phys. Rev. B* **1988**, *37*, 785.

(19) Becke, A. D. *J. Chem. Phys.* **1993**, *98*, 5648.

(20) Saunders, V.; Dovesi, R.; Roetti, C.; Orlando, R.; Zicovich-Wilson, C. M.; Harrison, N. M.; Doll, K.; Civalleri, B.; Bush, B.; D'Arco, P. L. M. *CRYSTAL 03 User's Manual*; University of Torino: Torino, 2003.

(21) Muscat, J.; Wander, A.; Harrison, N. M. *Chem. Phys. Lett.* **2001**, *342*, 397.

(22) http://www.tcm.phy.cam.ac.uk/~mdt26/basis_sets/Mo_basis.txt.

(23) http://www.crystal.unito.it.

(24) Kokalj, A. J. *Molec. Graph.* **1999**, *17*, 176.

(25) Basiev, T. T.; Sobol, A. A.; Voronko, Y. K.; Zverev, P. G. *Optical Mat.* **2000**, *15*, 205.

(26) Moura, M. R.; Guedes, I.; Grimsditch, M.; Loong, C. K. *J. Appl. Phys.* **2004**, *55*, 1448.

(27) Wood, D. L; Tauc, J. *Phys. Rev. B* **1972**, *5*, 3144.

(28) Longo, V. M.; Cavalcante, L. S.; Figueiredo, A. T.; de; Santos, L. P. S.; Longo, E.; Varela, J. A.; Sambrano, J. R.; Paskocimas, C. A.; De Vicente.; F. S; Hernades, A. C. *Appl. Phys. Lett.* **2007**, *90*, 091906.

(29) Eglitis, R. I.; Kotomim, E. A.; Bostel, G. *Eur. Phys. J. B* **2002**, *27*, 483.

(30) Eglitis, R. I.; Kotomim, E. A.; Bostel, G. *J. Phys.: Condens. Matter* **2002**, *14*, 3735.

(31) Laguta, V. V.; Rosa, J.; Zaritskii, M. I.; Nikl, M.; Usuki, Y. *J. Phys.: Condens. Matter* **1998**, *10*, 7293.

(32) Martini, M.; Meinardi, F.; Vedda, A.; Nikl, M.; Usuki, Y. *Phys. Rev. B* **1999**, *60*, 4653.

(33) Blistanov, A. A.; Zadneprovskii, B. I.; Ivanov, M. A.; Yakimova, I. O. *Cryst. Rep.* **2005**, *50*, 284.

(34) Sinelnikov, B. M.; Sokolenko, E. V.; Zvekova, E. G. *Inorg. Mater.* **1996**, *32*, 661.

(35) Lou, Z.; Cocivera, M. *Mater. Res. Bull.* **2002**, *37*, 1573.

(36) Laguta, V. V.; Martini, M.; Vedda, A.; Rosetta, E.; Nikl, M.; Mihokara, E.; Rosa, J.; Usuki, Y. *Phys. Rev. B* **2003**, *67*, 205102.

JP801587W